Journal of Cleaner Production 385 (2023) 135749

Contents lists available at ScienceDirect

Journal of Cleaner Production

journal homepage: www.elsevier.com/locate/jclepro

Revealing the impacts of human activity on the aquatic environment of the Pearl River Estuary, South China, based on sedimentary nutrient records

Rui Li [a,b], Zuobing Liang [a], Lei Hou [c], Di Zhang [d], Qirui Wu [a], Jianyao Chen [a,*], Lei Gao [b,**]

[a] School of Geography and Planning, Sun Yat-sen University, Guangzhou, 510275, China
[b] Key Laboratory of Vegetation Restoration and Management of Degraded Ecosystems, Chinese Academy of Sciences, South China Botanical Garden, Chinese Academy of Sciences, Guangzhou, 510650, China
[c] College of Ecology and Environment, Southwest Forestry University, Kunming, 650224, China
[d] Huizhou Hydrology Branch of Guangdong Provincial Hydrological Bureau, Huizhou, 516003, China

ARTICLE INFO

Handling Editor: Zhen Leng

Keywords:
Trophic state
Spatial distribution
Historical sedimentary record
Nutrient ratios
Reclamation

ABSTRACT

Elucidating environmental evolution and its influencing factors in estuarine areas is essential to coastal and marine ecological management. In this study, the spatiotemporal distributions of organic carbon (OC), total nitrogen (TN), total phosphorus (including geochemical speciation), $\delta^{13}C$ and nutrient ratios in sediments were explored to interpret changes in the aquatic environment of the Pearl River Estuary (PRE), and their sources in various periods were identified. Nutrients carried by surface runoff accumulated abundantly in the sediments of the northern and western shoals. Two dated sediment cores indicated a close relationship between environmental evolution in the PRE and the socioeconomic development of the Pearl River Delta (PRD). Rapid urbanization and population explosion in the PRD transformed the PRE from the pre-1970 low-impact state to a eutrophic state, which lasted until the end of the 1990s. After 2000, improvement of sewage treatment systems and environmental governance policies promoted the restoration of water quality, although inorganic nitrogen remained high in the coastal waters. Based on the threshold of sedimentary TN/OP ratio (5.60) of red-tide occurrence, the eastern shoal of the PRE exhibited high potential for red tides. Agricultural activities along the western coast lowered sedimentary OC/TN ratios (6.51 ± 1.54) near the river's outlets. The sedimentary $\delta^{13}C$ of organic matter (OM) in surface and subsurface sediments fell into the range of soil OM ($-25.46 \pm 0.82‰$), suggesting an expanding influence of eroded soil from land reclamation on Longxue Island. This research revealed the intense influence of human activities on the aquatic-environmental evolution and provides scientific basis for environmental restoration of the PRE in the future.

1. Introduction

An estuary is a transition zone between a river and the ocean, where strong saline-freshwater interactions occur that are affected by both terrestrial runoff and marine tides. The convenient transportation routes and superior ecological resources provide suitable conditions for rapid socioeconomic development in the estuarine deltaic region (Liu et al., 2021b). However, the urbanization process associated with continuous population growth imposes huge contamination loads on estuarine aquatic environments (Liu et al., 2005; Dai et al., 2011). Red tides triggered by excess accumulation of nutritive elements such as nitrogen and phosphorus sharply deteriorate water quality and threaten aquatic habitats (Sellner et al., 2003; Heisler et al., 2008; Conley et al., 2009). Moreover, toxic substances derived from harmful algal blooms (HABs) pose a risk to human health through bioaccumulation effects via food webs in areas used for aquaculture (Anderson et al., 2002).

Sediment acts as a major sink for terrestrial materials derived from rock weathering, soil erosion, atmospheric deposition and anthropogenic inputs, preserving a continuous record of regional environmental changes (Guo and Yang, 2016; Conrad et al., 2017; Irizuki et al., 2018; Velinsky et al., 2020; Liu et al., 2021a). Reconstruction of the aquatic environment based on radioactive isotope (e.g., ^{210}Pb and ^{137}Cs) chronology can provide sufficient supplements for areas lacking consistent long-term environmental monitoring data (Appleby, 2002). Jia and Peng (2003) found that the stable natural aquatic environment of the Pearl River Delta (PRD) had shifted to a human-disturbed system due

* Corresponding author.
** Corresponding author.
E-mail addresses: chenjyao@mail.sysu.edu.cn (J. Chen), gaolei@scbg.ac.cn (L. Gao).

https://doi.org/10.1016/j.jclepro.2022.135749
Received 18 August 2022; Received in revised form 9 December 2022; Accepted 24 December 2022
Available online 26 December 2022

mainly to economic development since the 1950s. Furthermore, water quality in this region deteriorated dramatically after 1990 as a result of rapid urbanization and industrial development, as supported by the historical chronology of core sediments from branches of the Pearl River (Gao et al., 2017; Li et al., 2019). However, reduced pollutant discharge relieved the accumulation levels of nutrients and heavy metals in sediments and enabled the gradual recovery of the overlying waters in recent years (Wang et al., 2015; Li et al., 2019; Ye et al., 2020).

Ratios of various nutritive elements can be used to identify the limiting factors for eutrophication and sources of nutrients during a certain historical period (Dai et al., 2007). Previous research has generally used the Redfield ratio (C: N: P = 106: 16: 1) to identify the limiting element for eutrophication (Redfield, 1958); however, this indicator is likely not suitable to estuarine areas due to the intense disturbance caused by terrestrial materials. Due to richness in protein and absence of cellulose, phytoplankton in marine systems typically has an OC/TN ratio between 4 and 10 (Jia and Peng, 2003), whereas terrestrial vascular plants universally have higher OC/TN ratio of 20 or greater (Meyers, 1994). Thus, this ratio has been widely applied to trace the origins of organic matter (OM) and to estimate the contributions of terrestrial and marine sources with pronouncedly different ratio ranges (Jia and Peng, 2003; Yu et al., 2010). Considering the different depletion rates of C and N during early diagenesis, utilizing only the OC/TN ratio may lead to misattribution of the OM source (Andrews et al., 1998). Integration of stable $\delta^{13}C$ and $\delta^{15}N$ isotope compositions into ratio methods can provide useful supplemental data for source apportionment of OM, as such isotopes can be used to effectively trace multiple sources and identify the predominant physicochemical processes (Collins et al., 2019; Xuan et al., 2020).

The PRD has become one of the most developed regions in China since the Chinese reform and opening-up policies were initiated in 1978. Over the past several decades, a large amount of domestic wastewater has been discharged into urban rivers, driven by a rapid increase in the local population (from 17.96 million in 1979 to 55.99 million in 2017) and poor efficiency of sewage treatment, leading to a massive input of nutritive substances into the Pearl River Estuary (PRE). In addition, more intense agricultural and maricultural activities have been noted as major drivers of severe eutrophication and frequent HABs (Huang et al., 2003; Hu et al., 2006). Meanwhile, P has been identified as the critical limiting factor for algal growth and reproduction in the PRE (Yin et al., 2000). More than 50 red tide events occurred during the period of 2001–2017 in Lingding Bay (a sub-estuary of the PRE; Marine Environment Bulletin of Guangdong Province, 2001–2017). However, detailed long-term observations of physicochemical properties in the PRE are not available, complicating analysis of the spatiotemporal characteristics of the eutrophication state and prediction of areas where red tide events are most likely to occur in the future. In this regard, the historical sequence contained in sedimentary records is an ideal complement for reconstructing the evolution of the aquatic environment. Moreover, nutrient ratios and stable isotopes may provide valuable information about the areas where red tide events are likely to occur. Thus, the aims of this research were: (1) to investigate the spatial distributions of nutrients and reconstructed historical changes in the aquatic environment; (2) to predict water areas with high potential for red tide; (3) to identify the potential sources of nutrients.

2. Materials and methods

2.1. Study area and sampling sites

The Pearl River, located in the subtropical region of South China, has a basin area of 4.54×10^5 km^2 and an average annual runoff of 3.38×10^{11} m^3. The river drains into Lingding Bay through four runoff outlets (Humen, Jiaomen, Hongqimen, Hengmen), where hydrological conditions vary spatially and seasonally due to interactions among riverine runoff, marine tides, and coastal currents. The PRE was formed from sediment carried by the second largest river in China and is surrounded by several megacities including Guangzhou, Shenzhen, Dongguan, Zhongshan, Zhuhai, Macau, and Hong Kong. Due to the demand for industrial and urban land, reclamation along the coast of the PRD has increased dramatically over the past three decades. On Longxue Island as an example, the land area has grown by more than 30 times as a result of a 30-year reclamation effort beginning in 1987 to support the construction of Guangzhou Harbor (Fig. 1c).

Nineteen sampling sites (LD1–LD19) were selected to represent the area most affected by human activities in the PRE and were classified into three categories based on their geographic positions and hydrological conditions: Category I included Sites LD1–LD6 near the outlets (Region I); Sites LD7–LD15 in the western region (Region II) were grouped into Category II; and Sites LD16–LD19 in the eastern region (Region III) were placed in Category III (Fig. 1b).

2.2. Collection and pretreatment of sediment samples

Sediment cores were collected during three sampling campaigns (August 2016, November 2017 and September 2018) using a gravity sampler at each site and stored in a plastic tube (6 cm diameter and 100 cm length) sealed with rubber plugs. After transportation to the laboratory, the cores were sliced at 1 cm intervals and gently homogenized via straining through a 1 mm nylon sieve after freeze-drying. The pretreated sediment samples were stored at −20 °C in the dark to measure particle size composition. The top 15 cm samples of the sediment cores were selected as the surface sediments.

2.3. Physicochemical properties of sediments

Sediment pH and electrical conductivity (EC) were measured in a 1:5 (*w/v*) ratio of dry sample to deionized water using a portable analyzer

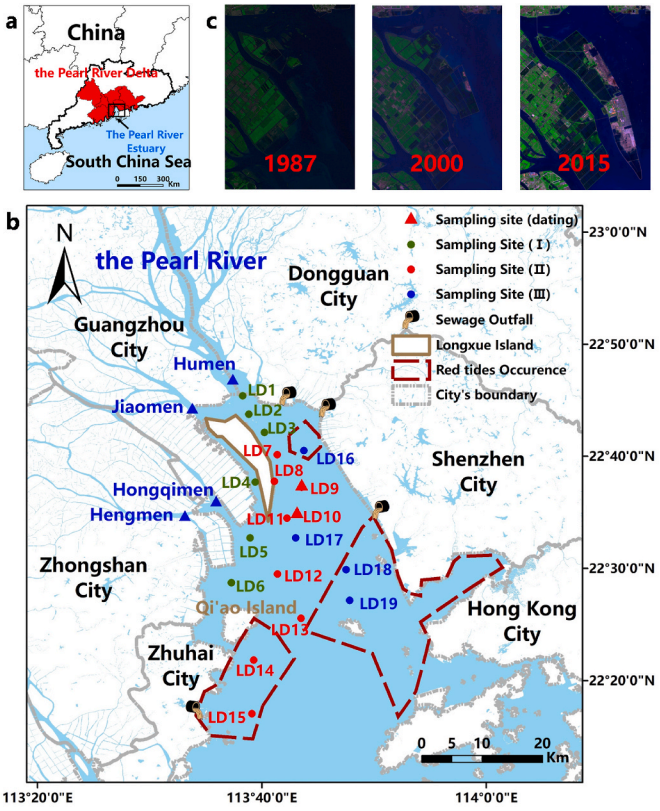

Fig. 1. Maps of the study area: (a) the Pearl River Delta and Lingding Bay located in southern China; (b) the map of sampling sites in Lingding Bay; (c) changes in the scope of Longxue Island from 1987 to 2015.

(LAQUAtwin; Horiba, Shanghai, China). After removal of OM and carbonates with 10% HCl and 10% H_2O_2, the particle size composition of sediment samples was analyzed with a laser particle size analyzer (Mastersizer 2000; Malvern Instruments, Malvern, UK). Then the sediment samples were ground with a mortar and pestle until all sediment particles passed through a 0.149 mm nylon sieve for subsequent chemical analysis. Approximately 40 mg sediment was acidified with 1 M HCl to remove carbonates and then dried at 60 °C to measure OC with an Elementar Vario TOC analyzer (Elementar Analysensysteme GmbH, Langenselbold, Germany). Next, 500 mg sediment was digested in H_2SO_4–$HClO_4$ mixture in a glass conical flask covered with a funnel, and the total concentration of phosphorus (TP) was determined using the molybdenum blue spectrophotometry method (Dick and Tabatabai, 1977). A sequential chemical extraction procedure was adopted to measure the loosely sorbed P (LS-P), iron-bound P (Fe–P), calcium-bound P (Ca–P), and organic P (OP) fractions in sediment (Hieltjes and Lijklema, 1980). The limit of detection (LOD) for dissolved phosphate in this series of analyses was 0.01 mg L^{-1}. TN was determined in the automated Kjeldahl analyzer (Kjeltec 8400, Foss, Denmark) after sediment samples were digested by concentrated sulfuric acid and catalyst (K_2SO_4: $CuSO_4$: Se = 100: 10: 1). Finally, 10% of all sediment samples were randomly selected for duplicate measurement, and the standard deviation of the analysis results was less than 10%.

Stable isotopic analysis ($\delta^{13}C$) of sediment was conducted using an elemental analyzer (Flash EA 2000, Thermo Fisher, USA) coupled with a mass spectrometer (Delta Advantage V, Thermo Fisher, USA). The detailed pretreatment and measurement procedures have previously been reported (Xuan et al., 2020). Stable isotope ratios are expressed in delta notation, as presented in Eq. (1):

$$\delta^{13}C(‰) = \left(\frac{R_{sample} - R_{standard}}{R_{standard}}\right) \times 1000 \quad (1)$$

where R_{sample} and $R_{standard}$ are the $^{13}C/^{12}C$ values of the sample and reference materials, respectively. The $\delta^{13}C$ values are reported relative to the Vienna PeeDee Belemnite standard (V-PDB). The analytical precision for $\delta^{13}C$ was 0.02‰.

2.4. Sediment ^{210}Pb chronology

Two long cores collected at sites LD9 (length: 70 cm) and LD10 (51 cm) were used for chronologic analysis of sediments. The radioisotope activities of ^{226}Ra and ^{210}Pb in cores LD9 and LD10 were measured using high-resolution γ-spectrometry with a high-purity germanium (HPGe) detector (GWL-120-15; ORTEC, Atlanta, GA, USA). Radioisotope activity determination of the sediment samples was conducted at the Nanjing Institute of Geography and Limnology, Chinese Academy of Sciences. Excess ^{210}Pb ($^{210}Pb_{ex}$) radioactivity was calculated by subtracting the supported ^{210}Pb radioactivity (determined from the ^{226}Ra activity) from the total ^{210}Pb radioactivity. The constant initial ^{210}Pb concentration (CIC) model was used to date the sediment profile (Appleby, 2002):

$$C_m = C_0 \bullet e^{-\lambda t} \quad (2)$$

where C_m and C_0 are the $^{210}Pb_{ex}$ radioactivities (Bq·kg^{-1}) at depth m and in surface sediments, respectively; λ is the decay constant of ^{210}Pb (0.03114 y^{-1}); and t is the time between the sedimentary age at depth m and in surface sediment (y).

The sedimentation rate in estuarine regions is generally high and shows large interannual variation. To reduce the uncertainty caused by the fluctuating sedimentation rate, a linear equation determined from logarithmic relationship of radioactivity with depth was used to calculate the mean sedimentation rate at a given time:

$$m = -\frac{s}{\lambda} ln[C(m)] + \frac{s}{\lambda} ln[C(0)] \quad (3)$$

$$s = -\lambda \bullet k \quad (4)$$

$$S = s \bullet \gamma \quad (5)$$

where k is the slope of the linear equation, s is the sedimentation rate (cm·y^{-1}), and S is the sedimentation flux (g·cm^{-2}·y^{-1}).

2.5. Statistical analysis

Kolmogorov-Smirnov Test was applied to test the normality of variables. Differences among sampling sites were analyzed using one-way analysis of variance (ANOVA) with a significance level of 0.05, and Levene's test was applied to test the homogeneity of variance. Pearson's correlation was used to identify relationships between variables, and correlations were considered significant at $p < 0.05$. All statistical analyses were performed using IBM SPSS software (ver. 22.0; SPSS, Armonk, NY, USA). The spatial interpolation diagrams for TN/OP and OC/OP were drawn in ArcGIS (ver. 10.2; ESRI, Redlands, California, USA) using Kriging interpolation method.

3. Results and discussion

3.1. Physicochemical properties of sediment

The basic physicochemical properties of the analyzed sediments are summarized in Table 1. Sediments were slightly alkaline, with average pH values ranging from 7.30 to 8.38. EC values were lower in region I (mean: 0.63–1.10 mS cm^{-1}) than in regions II and III (mean: 1.44–2.71 mS cm^{-1}) ($p < 0.05$), mainly due to the dilution effect caused by freshwater runoff (Table S1). The fine particle component (FPC), consisting of clay and silt (<63 μm), was the dominant grain fraction (mean: 84.74–99.09%) in surface sediments in region II, suggesting relatively stable depositional conditions. Meanwhile, sediments in regions I and III contained abundant sand, with average FPC values in the ranges of 48.98–96.06% and 26.98–85.76%, respectively. The distribution pattern of sediment particle size is associated mainly with specific hydrological regimes and topographic conditions in the PRE. The fast velocity and changeable direction of water flow near the outlet of the Pearl River limits the deposition of fine suspended particulates. Affected by the Coriolis force, suspended matter originating from freshwater runoff is transported with the discharge of the Pearl River toward the South China Sea (SCS) along the west shoal during the ebb tide (Zhou et al., 2004). With the weakened influence of riverine runoff during the flood tide or dry season, massive coarse grains produced through hydraulic erosion are carried with tidal currents and ultimately deposited along the eastern coast (Zhang et al., 2019). As a result, differences in the distribution pattern of sediment particle size may lead to heterogeneity in the spatial distribution of nutrients in the PRE.

3.2. Spatial distribution of nutrients in surface sediments

Overall, nutritive substances (OC, TN, and TP) were positively related to FPC ($p < 0.05$) (Table 2), demonstrating a particle-size-dependent spatial distribution pattern of sediments in the PRE. TP concentrations in surface sediments were significantly higher in regions I and II (mean: 0.52–0.9 g kg^{-1}) than in region III (mean: 0.38–0.62 g kg^{-1}) ($p < 0.05$), with the highest values observed at site LD2 (0.90 ± 0.14 g kg^{-1}), near the Humen outlet (Table 1 and Table S1). This finding is in accord with previous research (Zhang et al., 2019). The geochemical fractions of phosphorus in sediments are shown in Fig. S1. OP was the dominant fraction, with concentrations ranging from 0.08 to 0.57 g kg^{-1}, accounting for 44.67–68.38% of TP. Inorganic P (mainly reactive orthophosphate) is readily adsorbed onto suspended particles (Jordan et al., 2008), leading to great potential for nearshore deposition. LS-P (<0.01–0.02 g kg^{-1}) and Fe–P (0.03–0.42 g kg^{-1}) are generally

Table 1
Physicochemical properties of the surface sediment.

Site		pH	EC ($mS•cm^{-1}$)	FPC (%)	Ca (%)	TP ($g•kg^{-1}$)	OC ($g•kg^{-1}$)	TN ($g•kg^{-1}$)	OC/TN	$\delta^{13}C$ (‰)
		n = 15	n = 15	n = 15, %	n = 15	n = 15	n = 15	n = 4	n = 4	n = 1
Region I (close to outlets)	LD1	7.30 ± 0.19	1.10 ± 0.43	80.18 ± 5.97	0.20 ± 0.03	0.60 ± 0.07	6.84 ± 0.72	0.81 ± 0.18	10.65 ± 1.20	−25.32
	LD2	7.43 ± 0.13	0.94 ± 0.29	91.74 ± 6.17	0.29 ± 0.07	0.90 ± 0.14	11.71 ± 1.42	1.07 ± 0.19	13.44 ± 1.10	−25.12
	LD3	7.32 ± 0.18	0.96 ± 0.25	91.72 ± 3.77	0.23 ± 0.06	0.61 ± 0.04	7.60 ± 0.54	0.78 ± 0.14	11.59 ± 1.77	−25.40
	LD4	7.81 ± 0.10	0.63 ± 0.18	48.98 ± 13.87	0.33 ± 0.18	0.52 ± 0.06	5.33 ± 0.81	1.00 ± 0.28	6.63 ± 2.08	−25.47
	LD5	7.99 ± 0.07	0.70 ± 0.04	89.58 ± 8.60	0.63 ± 0.06	0.76 ± 0.08	5.11 ± 0.54	0.87 ± 0.12	6.76 ± 0.35	−26.52
	LD6	8.01 ± 0.06	0.80 ± 0.07	96.06 ± 1.85	0.53 ± 0.08	0.70 ± 0.03	5.08 ± 0.33	1.06 ± 0.34	6.16 ± 0.35	−25.72
Region II (western shoal)	LD7	7.71 ± 0.05	1.95 ± 0.06	85.50 ± 3.60	0.14 ± 0.05	0.50 ± 0.03	6.48 ± 0.34	0.83 ± 0.11	9.25 ± 1.42	−25.14
	LD8	7.53 ± 0.16	1.98 ± 0.20	86.67 ± 5.81	0.26 ± 0.11	0.56 ± 0.05	8.72 ± 0.76	1.09 ± 0.11	9.57 ± 0.38	−25.00
	LD9	8.00 ± 0.06	2.71 ± 0.20	99.09 ± 1.25	0.20 ± 0.06	0.62 ± 0.05	8.74 ± 0.45	1.45 ± 0.08	6.77 ± 0.28	−26.09
	LD11	8.06 ± 0.09	1.44 ± 0.17	84.74 ± 6.44	0.49 ± 0.14	0.66 ± 0.04	8.63 ± 0.85	1.13 ± 0.14	9.15 ± 1.37	−23.08
	LD10	7.78 ± 0.11	1.75 ± 0.23	87.09 ± 6.42	–	0.69 ± 0.04	7.82 ± 1.02	0.97 ± 0.11	10.10 ± 1.29	−25.03
	LD12	7.98 ± 0.11	1.67 ± 0.27	90.67 ± 9.12	0.49 ± 0.08	0.68 ± 0.06	4.87 ± 0.55	0.79 ± 0.19	7.71 ± 1.88	−25.87
	LD13	8.38 ± 0.05	2.07 ± 0.09	91.60 ± 7.39	0.42 ± 0.14	0.68 ± 0.05	4.66 ± 0.38	1.01 ± 0.05	5.49 ± 0.19	−23.81
	LD14	8.26 ± 0.07	1.47 ± 0.16	96.98 ± 2.76	0.47 ± 0.14	0.75 ± 0.08	4.56 ± 0.20	1.05 ± 0.10	5.30 ± 0.46	−24.91
	LD15	8.26 ± 0.07	2.05 ± 0.12	98.34 ± 0.81	0.36 ± 0.07	0.71 ± 0.06	4.30 ± 0.32	0.88 ± 0.28	6.17 ± 2.09	−25.34
Region III (eastern shoal)	LD16	7.88 ± 0.11	1.60 ± 0.11	26.98 ± 5.68	0.30 ± 0.14	0.38 ± 0.06	2.26 ± 0.47	0.86 ± 0.32	3.88 ± 1.46	−25.74
	LD17	7.93 ± 0.09	1.67 ± 0.14	34.12 ± 15.46	0.29 ± 0.11	0.40 ± 0.14	2.14 ± 1.03	0.46 ± 0.09	5.56 ± 2.90	−27.06
	LD18	8.06 ± 0.24	2.25 ± 0.26	85.76 ± 8.88	0.18 ± 0.09	0.49 ± 0.07	3.32 ± 0.82	0.67 ± 0.20	5.81 ± 1.81	−26.23
	LD19	8.38 ± 0.16	1.88 ± 0.40	66.11 ± 23.71	0.19 ± 0.05	0.44 ± 0.16	3.33 ± 1.40	0.76 ± 0.09	4.63 ± 2.13	−26.66

Data expression: mean ± standard deviation.
FPC indicates the component of sediment particle with diameter <63 μm.

Table 2
Correlation between the physicochemical properties of the surface sediments (n = 285).

	pH	EC	FPC	Ca	TP	OC	TN
pH	1	**0.333****	**0.245****	**0.338****	0.095	**−0.535****	0.094
EC		1	**0.255****	**−0.294****	**−0.203****	−0.108	−0.020
FPC			1	**0.208****	**0.666****	**0.318****	**0.337****
Ca				1	**0.460****	−0.080	0.193
TP					1	**0.419****	**0.359****
TOC						1	**0.494****
TN							1

** and * represent significant correlation at $p < 0.01$ and 0.05, respectively.

considered the labile fraction associated with anthropogenic inputs (Roy et al., 2017), contributing 0.03–3.07% and 13.29–39.86% of TP, respectively. LS-P exhibits high mobility in aquatic environments, whereas Fe–P tends to be released due to reductive dissolution of Fe oxides under oxygen-deficient conditions (Ding et al., 2016; Parsons et al., 2017). Thus, sediments with high concentrations of labile P fractions in regions I and II showed the greatest potential for remobilization in the PRE. Ca–P (8.96–32.13%), mainly composed of apatite and phosphate adsorbed on $CaCO_3$, was in the range of 0.02–0.17 g kg^{-1}. Ca–P originates mainly from the weathering of sedimentary deposits; this fraction is stable under the alkaline conditions (Hieltjes and Lijklema, 1980; Golterman, 2007). Regions I and II generally had higher Ca–P concentrations than region III (Fig. S1) due to the significantly lower ($p < 0.05$) Ca content in region III (Table S1).

As shown in Table 1, mean concentrations of OC and TN in surface sediments were in the ranges of 2.14–11.71 g kg^{-1} and 0.46–1.45 g kg^{-1}, respectively; these concentrations were significantly higher in regions I and II than in region III ($p < 0.05$), mainly due to the higher FPC proportions of sediments in regions I and II (Table S1), as such sediments have greater specific area and provide more adsorption sites for nutrients (Zhang et al., 2020). OC and TN concentrations in the surface sediments of regions I–III were generally lower than reported concentrations observed before 2010 (Table S2) (Jia and Peng, 2003; Hu et al., 2006; Zhang et al., 2009a). Sediment OC and TN concentrations

were previously reported as 11 and 1 g kg^{-1}, respectively, in the freshwater–brackish water transition area (Yu et al., 2010). This discrepancy demonstrates that nutrient concentrations in the deposited particles have undergone distinct changes over the past decade. Thus, to better understand changes in the eutrophic state of the aquatic environment in the PRE, an in-depth investigation of the historical variation in nutrient concentrations in sediment cores is needed.

3.3. Chronology and sedimentation condition

As illustrated in Fig. 2, profiles of $^{210}Pb_{ex}$ radioactivity in sediment cores LD9 and LD10 showed a monotonically decreasing trend with depth, indicating a sequential and relatively stable depositional environment (Bing et al., 2016). Given that the minimum $^{210}Pb_{ex}$ radioactivities in LD9 and LD10 were much greater than 0, utilization of the CRS (constant rate of ^{210}Pb supply) model may cause overestimation of sedimentary age for the bottom sediments (Appleby, 2002). Thus, the CIC model was employed to establish linear regressions between logarithmic $^{210}Pb_{ex}$ activity and depth. Then the sedimentary records were reconstructed, creating a 59-year history for LD9 (corresponding to 1959–2017) and 34-year history for LD10 (1983–2016) with mean sedimentation rates of 1.19 and 1.50 cm y^{-1}, respectively (Fig. 2). These rates are roughly in accord with previous reports in the PRE. The sedimentation fluxes in this study (0.65 g $cm^{-2}{\cdot}y^{-1}$ for LD9 and 1.25 g $cm^{-2}{\cdot}y^{-1}$ for LD10) were higher than reported values on the eastern shoal (0.458 and 0.59 g $cm^{-2}{\cdot}y^{-1}$) and lower than previous reports on the western shoal (1.13–1.55 g $cm^{-2}{\cdot}y^{-1}$) (Jia and Peng, 2003; Ip et al., 2004; Zhang et al., 2009a; Ye et al., 2012). These results indicate that the western shoal, particularly the area near Qi'ao Island, is the main depositional area due to the combined effects of terrestrial runoff discharge, tides, coastal currents, and topographic conditions (Zhou et al., 2004; Zhang et al., 2019).

3.4. Aquatic environment reconstruction based on historical variation in nutrients

OC, TP, and TN concentrations in core LD10 were in the ranges of 5.70–11.81 g kg^{-1}, 0.58–0.78 g kg^{-1}, and 0.53–1.30 g kg^{-1}, respectively (Fig. 3b). Meanwhile, these concentrations were in the ranges of 6.94–11.31 g kg^{-1}, 0.51–0.90 g kg^{-1}, and 0.45–1.67 g kg^{-1} in core LD9 (Fig. 3a). According to the vertical profiles of nutritive substances in the two sediment cores used for dating, historical variation patterns of the aquatic environment in the PRE can be divided into four stages.

Period I (before 1970), corresponding to 55–70 cm in LD9, had lower anthropogenic impacts and was characterized by relatively low nutrient levels, with average OC, TP, and TN concentrations of 7.68, 0.58, and 0.88 g kg^{-1} (Fig. 3a and Fig. S2).

In Period II (1971–1984), corresponding to the depth range of 40–55 cm in LD9 (Fig. 3a). Sediment TP concentrations increased from 0.61 g kg^{-1} in 1971 to 0.86 g kg^{-1} in 1984 monotonically, while OC concentrations increased from 7.95 g kg^{-1} in 1980 to 10.80 g kg^{-1} in 1984 rapidly (Fig. 3a). Assuming that OC input from natural sources was constant over time, the augmentation of sediment OC was associated mainly with the anthropogenic inputs and represents the increasing impacts of human activities. The second baby boom in China occurred in 1962–1970 (Jiang, 1995), which induced an explosion in the working-age population (age range: 15–64) over the following 10–20 years and subsequently increased the discharge of sewage into the PRE. And a drastically increasing trend of chemical fertilizer application from 1971 (1.52×10^5 ton) to 1984 (3.79×10^5 ton) was responsible principally for the increase in nutrients load (Fig. S2).

Period III (1985–2000) corresponded to the depth range of 20–40 cm in LD9 and 18–51 cm in LD10 (Fig. 3). During this stage, OC, TP, and TN concentrations remained high, with average concentrations of 8.83, 0.68, and 0.94 g kg^{-1} in LD10, respectively, and slightly higher levels in LD9 (9.78 g kg^{-1}, 0.78 g kg^{-1}, and 1.25 g kg^{-1}, respectively) (Fig. 3). Since the Chinese reform and opening-up policies were enacted in 1978, the PRD has become one of the fastest-developing regions in China. Though the application of chemical fertilizer increased slightly, the population expansion in the PRD was main cause for sharp increases in sewage discharge and contamination loads to the estuarine waters (Fig. S2) (Gao et al., 2017; Li et al., 2019). In addition, flourishing aquaculture in the PRD began to directly introduce nutrients from excess feed and excrement into the estuary in the early 1990s (Wang et al., 2015). The significant positive relationships ($p < 0.05$) between OC, TN, TP and socioeconomic indexes (except TP and GDP) from 1971 to 2000 indicated that intense human activities have led to eutrophication in the PRE (Table S5).

Period IV (after 2000) corresponded to the top 20 cm in LD9 and top 18 cm in LD10 (Fig. 3). TP concentrations showed upward decreasing trends and OC concentrations were lower than Period III in the two sediment cores, suggesting reductions in anthropogenic inputs of OM and P. Improved water quality in the PRE has been reported in previous researches (Wang et al., 2015; Zhao et al., 2020). A significant negative relationship ($p < 0.01$) between TP and domestic sewage treatment rate highlighted the contribution of the latter to reduction in P loads (Table S5). In contrast to OC and TP, TN concentrations remained stable at high levels with some fluctuations in both LD9 (mean value: 1.37 g kg^{-1}) and LD10 (mean value: 0.92 g kg^{-1}) over recent years (2000–2017). It seemed that TN loads were less influenced by the promotion of domestic sewage treatment rate (Table S5) due mainly to nitrogen removal is still the bottleneck of sewage treatment processes in China (Chen et al., 2022). According to monitoring data from the Department of Ecology and Environment of Guangdong Province (2015–2017), concentrations of inorganic nitrogen have remained high in the overlying water of the PRE in recent years (Table S4), exceeding environmental quality standards for surface water (Class III) (1 mg L^{-1} as total N) (GB 3838–2002) at most sampling sites, although inputs of phosphate had already been effectively reduced. The abundant nitrogen in the aquatic environment enabled P to become the limiting factor for eutrophication in the PRE (Yin et al., 2000; Huang et al., 2003). P is an important nutritive element that regulates primary productivity by playing an essential role in the material and energy conversion process of photosynthesis as a vital component of the chloroplast and adenosine triphosphate (Canfield et al., 2005). Thus, sedimentary P is an important proxy for the eutrophication state of the aquatic environment.

The geochemical fractions of phosphorus were employed for interpretation of the historical changes in eutrophication state and the environmental evolution of the PRE (Fig. 4). The sum of Ca–P and OP concentrations showed little change throughout the profile (Fig. S3), while labile P (LS-P and Fe–P) concentrations had similar variation

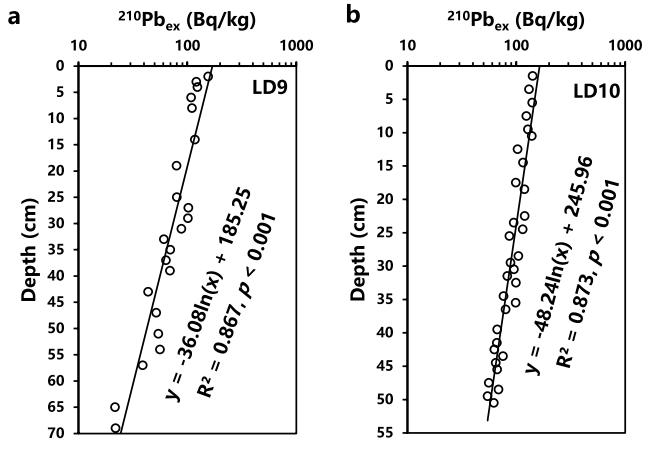

Fig. 2. Vertical profiles of $^{210}Pb_{ex}$ radioactivity in sediment cores (a) LD9 and (b) LD10.

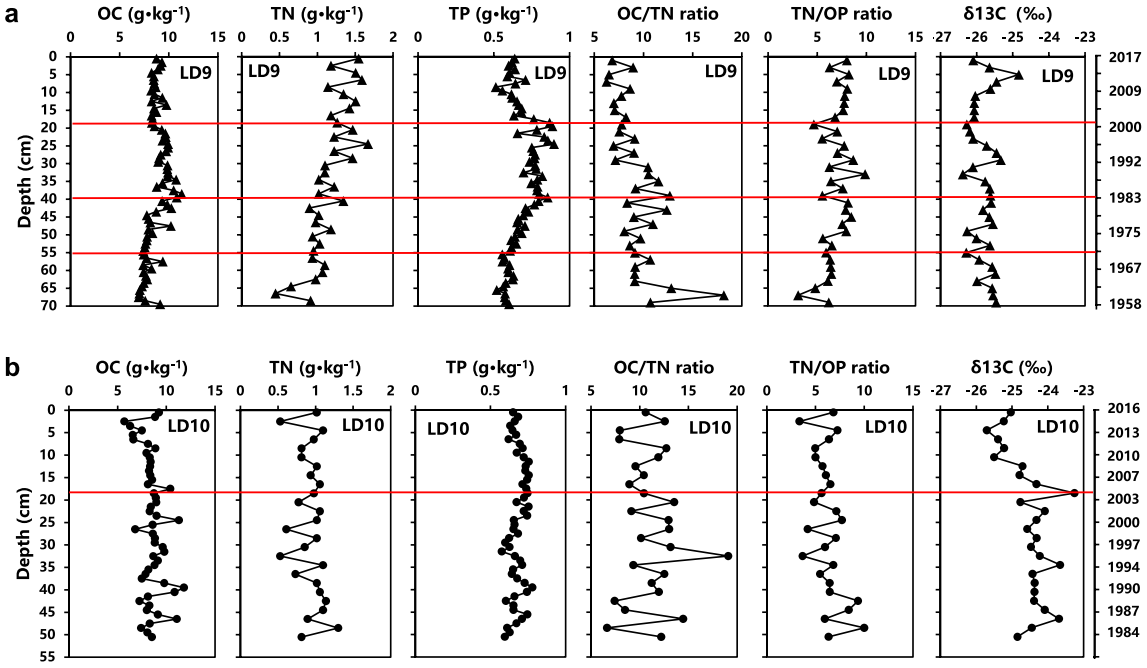

Fig. 3. Vertical profiles of OC, TN, TP, OC/TN ratio, TN/OP ratio and $\delta^{13}C$ in sediments cores LD9 (a) and LD10 (b).

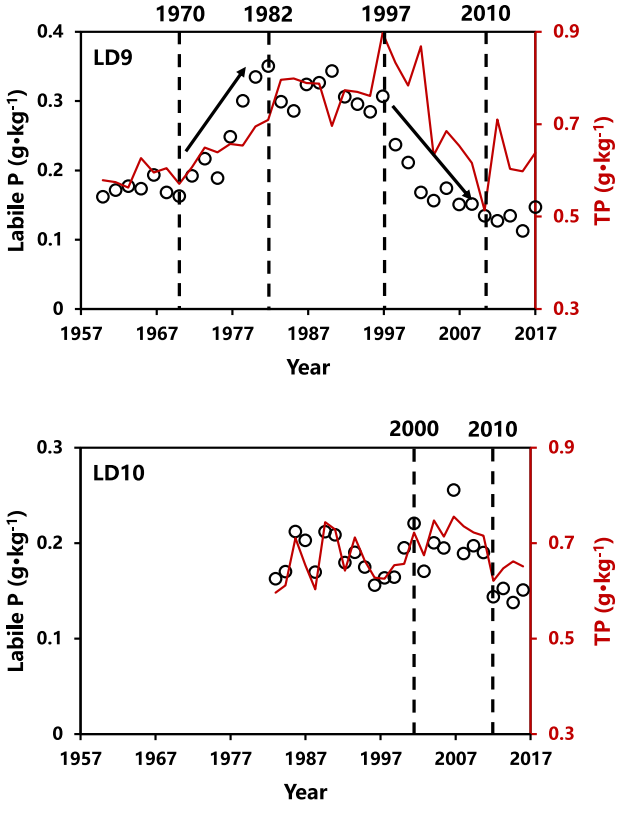

Fig. 4. The temporal variation of labile P concentration (black hollow circle) and TP concentration (red line) in sediment cores LD9 and LD10.

patterns to TP concentrations (Fig. 4). In Period I, low labile P concentrations (mean: 0.17 g kg^{-1}) in sediments indicated a state of limited anthropogenic inputs. Then the PRE experienced a dramatic increase in exogenous P input during the rapid development of the PRD during Periods II and III (Fig. 4). Notably, labile P had a significant positive relationship ($p < 0.05$) with fertilizer application but weakly associated with other socioeconomic indexes (Table S5), suggesting that the increase in TP was driven mainly by the increase in application rate of agrochemicals. At site LD9, labile P concentrations began to decrease around 2000, and water quality approached background levels after 2010. However, the changing trend at site LD10 was not obvious, and labile P concentrations (mean: 0.18 g kg^{-1}) in period III was lower than those at LD9 (mean: 0.29 g kg^{-1}) (Fig. 4), which indicated less impact from anthropogenic input on site LD10. According to statistical yearbooks, the upgrade and improvement of the municipal water pollution treatment system commenced in the early 2000s in the PRD (Fig. S2). Therefore, nutrient loads discharged into the aquatic environment showed a pronounced reduction despite the resident population of PRD cities increasing by about 1.2 times, which increased the production of domestic sewage during this period (Fig. S2). In recent years, strict regulation measures such as the River Chief System have markedly reduced exogenous nutrient inputs into the PRE, promoting the restoration of water quality in the Pearl River System (Liu et al., 2019).

Restoration of the aquatic environment from eutrophication has been observed in coastal areas of developed countries that experienced environmental contamination associated with development earlier than the PRD (Velinsky et al., 2020). However, a reduction in nutritive elements does not always benefit aquatic ecosystems. For example, the rapid oligotrophication process caused by reducing phosphorus loads to the Seto Inland Sea disrupted the balance of nutrients, which altered the species composition of phytoplankton, thereby reducing the fishery production (Yamamoto, 2003; Irizuki et al., 2018). In the PRE, reduction of phosphate despite the presence of high levels of inorganic nitrogen would likely have negative effects on the nutrient structure of the aquatic environment (Table S4). The main class of red-tide-causing organisms was diatom between 2001 and 2003 and then shifted to *Dinoflagellata* after 2006 according to the Marine Environment Bulletin of Guangdong Province (2001–2017) (Table S6). This transformation likely had long-lasting impacts on the aquatic ecosystem through effects on the food web. Therefore, both nutrient concentrations and nutrient ratios should be considered in environmental management.

3.5. Nutrient ratios and eco-environmental implications

Nutrient ratios are good indicators of sediment provenance and diagenetic alteration to reveal the eco-environmental changes in the overlying water (Dai et al., 2007; Canfield et al., 2020). As shown in Fig. 5, the TN/OP and OC/OP ratios of surface sediments (4.2–10.8 and 36–53, respectively) were markedly lower than values based on the Redfield ratio (16 and 106) (Redfield, 1958). According to the Marine Environmental Bulletin of Guangdong Province (2001–2017), red tides mainly occurred along the coasts of Zhuhai City and Shenzhen City (Fig. 1b), which roughly aligned with the water areas that had sedimentary TN/OP ratios higher than 5.60 (Fig. 5). Since P is the main limiting factor for algae growth (Yin et al., 2000), that value can be considered an important threshold controlling red-tide development. OC/OP ratios decreased with increasing distance from the outlet of the Pearl River, and this distribution pattern is likely related to the typically greater OC/OP ratios of terrestrial OM (Sterner and Elser, 2003).

Nutrient ratios also showed marked historic variation in the studied sediment cores (Fig. 3). Before the 1970s, the TN/OP ratio had a mean value of 5.48, below the red-tide threshold (5.60), which generally increased after 1975 and peaked in 1990 (9.87) (Fig. 3a), aligning with the timeline of frequent red tide events since the 1980s (Qian and Liang, 1999; Zhang et al., 2009b). Since 2000, low sedimentary TN/OP ratios (5.82 ± 1.09) have been recorded in core LD10 and higher values (7.20 ± 1.00) have been found in core LD9, suggesting notable regional features of red-tide events in the PRE.

3.6. Source analysis based on element ratios and $\delta^{13}C$

Differentiation of terrestrial and endogenous OM is conducive to interpreting the factors underlying the spatiotemporal distribution of nutritive elements in the PRE. As shown in Fig. 3, the OC/TN ratios of sediment cores LD9 and LD10 were 9.23 ± 2.30 and 11.09 ± 2.62, respectively, and were generally higher than the Redfield ratio (Redfield, 1958). In core LD10, OC/TN ratios fluctuated throughout the whole profile without an obviously changing trend. In core LD9, this value was high from 1965 to 1988 recording the high proportion of land-derived OM during Periods II and III, and then that decreased to a value (6.81) close to the Redfield ratio in surface sediments. Decreasing OC/TN ratios in the upper sediments validated the decrease in land-derived OM since 2000. However, the abnormally high OC/TN ratios of 18.19 and 19.08 observed at the depth of 67 cm in core LD9 and at the depth of 33 cm in core LD10, respectively, was likely attributable to substantial loss of N caused by the preferential degradation of N-enriched OM (Jia and Peng, 2003). In surface sediments, mean OC/TN ratios were in the range of 3.88–13.44 (Table 1). Sediments collected from the eastern stream (e.g., sites LD1, LD2, LD3, LD7, LD8, LD10, and LD11) had much higher OC/TN ratios (mean: 9.15–13.44) than those from other regions due to the discharge of land-based OM via the Humen outlet. Although sites LD4, LD5, and LD6 were near the other three outlets (Jiaomen outlet, Hengmen outlet, Hongqili outlet), OC/TN ratios were lower and close to the Redfield ratio (~6.7) (Redfield, 1958). This result is coincident with a previous report of a decreasing OC/TN ratio from the pristine upstream section in a natural reserve (11.8) to the PRE (5.0) (Liu et al., 2020). This decrease in OC/TN ratio was attributed to N-enriched wastewater discharged along the western coast, where cropland is the dominant land-use type (Fig. S4). In humid regions, more than 20% of nitrogen fertilizers applied to farmland can be discharged into river systems with rainfall (Kabir et al., 2021), and are ultimately transported to estuarine waters. Therefore, the OC/TN ratio is likely to provide inaccurate assessments in estuarine regions severely influenced by terrestrial materials with low OC/TN ratios that undergo rapid mineralization after burial in sediments.

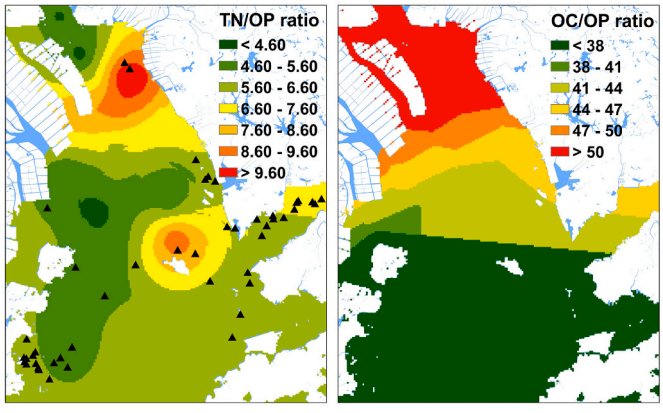

Fig. 5. TN/OP and OC/OP ratios of the surface sediments in the Pearl River Estuary [Black triangle represents the general locations of red-tide events recorded by the Marine Environmental Bulletin of Guangdong Province (2001–2017)].

As robust supplemental data, $\delta^{13}C$ values of sediments in this study and previous reports are presented in Fig. 3 and Table 1 and Table S7 (Jia and Peng, 2003; Yu et al., 2010; Xuan et al., 2020). Contributions from C4 plants can be excluded from these data, as the natural ecosystem of the PRD is predominated by subtropical forest and the main cultivated plant is rice (Jia and Peng, 2003). Thus, land-derived OM from both natural and anthropogenic sources had much lower $\delta^{13}C$ values than algal OM. In the PRE, $\delta^{13}C$ values of OM were higher in the surface sediments of region II (−24.67 ± 0.94‰) than regions I (−25.59 ± 0.45‰) and III (−25.99 ± 0.70‰) (Table 1), indicating a larger contribution from terrestrial OM near the outlets and eastern shoal. The discharge of domestic sewage from coastal cities is likely a major source of sedimentary OM in the eastern region. In addition, large areas of mangroves are distributed around Shenzhen Bay and Hong Kong City, and their debris can be carried on coastal currents and settle on the eastern shoal, decreasing $\delta^{13}C$ values.

The $\delta^{13}C$ values were in the ranges of −26.38‰ to −24.83‰ in core LD9 and –25.71‰ to −23.26‰ in core LD10 (Fig. 3). These values fell within the range between marine phytoplankton (−22‰ to −20‰) and terrestrial OM (−29.9‰ to −25.46‰) (Table S7), indicating combined impacts on estuarine sediments. Compared to LD10, lower $\delta^{13}C$ values in LD9 represented a greater contribution of land-derived OM to sediments, corresponding to the higher input of anthropogenic P in Period III (Fig. 4). The two sediment cores showed different trends of $\delta^{13}C$ values over the past two decades. The increase in $\delta^{13}C$ values at 5–11 cm depth in LD9 indicated reduced inputs of terrestrial OM between 2008 and 2013. Meanwhile, $\delta^{13}C$ values in LD10 showed a monotonically decreasing trend after 2003, and then stabilized at low values after 2010 (mean: 25.35 ± 0.22‰), corresponding to the depth range of 0–10 cm. This value is comparable to that of soil OM (−25.46 ± 0.82‰) in the PRD (Table S7) (Xuan et al., 2020). The same decreasing trend of $\delta^{13}C$ values was observed in the top layers of LD9, where $\delta^{13}C$ values also fell within the range of soil OM. The land reclamation project on Longxue Island, which was launched in 1987 and has accelerated since 2000, was likely a key factor reducing $\delta^{13}C$, as eroded soil with low $\delta^{13}C$ values was deposited in the top sediment layers. This possibility was confirmed by the $\delta^{13}C$ values of surface sediments collected near the island being similar to soil OM, e.g., LD4 (−25.47‰), LD7 (−25.14‰), and LD8 (−25.00‰). Notably, there is a lag of approximately 10 years in the temporal trends of sediment $\delta^{13}C$ between cores LD9 and LD10. This lag was likely affected by the ongoing impact of land reclamation on the aquatic environment of the PRE.

3.7. Lessons from aquatic-environment evolution in the PRE

The estuaries around world are all affected by human activities to different extent, mainly depending on the development level of the surrounding regions (Dai et al., 2007, 2011; Conrad et al., 2017). The

PRD, one of the fastest developing regions in the human history, produced massive nutrient loads in the estuarine regions, resulting in eutrophication and subsequent red tides. Encouragingly, the restoration signals of water quality from eutrophication occurred earlier after the application of reasonable and effective pollution prevention and control measures in the PRE compared with other developed estuaries worldwide (Fig. 4, Fig. S2, Table S5 and Table S8) (Andrén et al., 2017; Ellegaard et al., 2006; Irizuki et al., 2018; Koster et al., 2007; Li et al., 2015). In-time establishment of the sewage treatment system efficiently reduced OC & TP loads deriving from point-source pollutant, which could be a good example of environmental management to follow in other developing regions.

Notably, the reductions in P and N were not synchronized, and the latter mainly originated from the agricultural non-point source pollution still remained at high levels, potentially disrupting the nutrient balance of coastal waters (Figs. 3 and 5, Fig. S4 and Table S4). Therefore, improvement of farming practices such as accurate calculation of agrochemical nitrogen and cultivation of cover crops is a priority in coastal cities, even in the whole river basin. Meanwhile, nutrient management plans involving farmers, the public and the government has played a key role in reduction of nitrogen loads in many estuaries and is a worthwhile strategy for future environmental management in the PRE (Beegle et al., 2000; Greening et al., 2014; Némery and Garnier, 2016). In addition, aquaculture of bivalve mollusks may be an economical method for N removal from water environment (Bricker et al., 2018, 2020). Another potential risk is caused by construction program of large-sized port and land reclamation project in coastal areas, which result in more transportation of terrigenous materials into the estuary (Figs. 1 and 3). Over-development of coastlines is always accompanied by pollution and ecological degradation (de Mulder et al., 1994; Lee et al., 2014), consequently, implementation of pivotal scientific strategies including adequate pre-planning, strict control of scale, establishment of red line setting, development of artificial wetland, and improvement of land reclamation methods are recommended to reduce the adverse impacts. With regard to the reclamation project, application of cleaning landfill materials needs to be prioritized. The contradiction between economic development and environmental protection existed in the past development mode, therefore, appropriate adjustment and implementation of policies, laws and regulations are important guarantees to reduce the anthropogenic impacts on the estuarine environment.

4. Conclusions

In the PRE, high levels of nutritive elements (C, N, and P) have accumulated in the sediments of the western and northern shoals, mainly due to hydrodynamic and topographic conditions. The historical changing trends of the aquatic environment were closely associated with human activities and could be divided into four stages: before 1970, the aquatic environment was rarely affected by anthropogenic inputs; then, population growth and urbanization in the PRD from 1971 to 1983 gradually increased the discharge of sewage into the PRE until the late 1990s; since 2000, OC and P loadings have been markedly reduced due to improvement of the sewage treatment system. However, N levels have remained high, leading to a risk for nutrient imbalance, possibly transforming the community structure of algae, and altering the food web. Coastal areas near Zhuhai City, Dongguan City, and Shenzhen Bay had higher sedimentary TN/OP ratios and greater potential for red-tide development. In addition, N-enriched OM from agricultural activities decreased sedimentary OC/TN ratios near outlets of the Pearl River. The $\delta^{13}C$ values of surface sediments indicated that land reclamation on Longxue Island led to settling of more eroded soil around the island. In environmental management strategies, the nutrient structure of the water body and the protection of natural coastlines should be considered.

Author contribution statement

Rui Li: Conceptualization, Investigation, Methodology, Writing-original draft, Writing-review & editing, Formal analysis. Zuobing Liang: Investigation, Experimental analysis. Lei Hou: Investigation, Funding acquisition. Di Zhang: Experimental analysis. Qirui Wu: Investigation, Experimental analysis. Jianyao Chen: Conceptualization, Writing-review & editing, Validation, Funding acquisition. Lei Gao: Conceptualization, Methodology, Investigation, Writing-review & editing, Funding acquisition, Validation.

Declaration of competing interest

The authors declare that they have no known competing financial interests or personal relationships that could have appeared to influence the work reported in this paper.

Data availability

The authors are unable or have chosen not to specify which data has been used.

Acknowledgements

The authors are very grateful to Jun Wang from Sun Yat-sen University for providing the land use type data and reviewers for providing invaluable suggestion and comment. This work was financially supported by the National Natural Science Foundation of China (Project No. 42077376 and 41961144027), the Youth Innovation Promotion Association CAS (2022352), the Foundation of Key Laboratory of Vegetation Restoration and Management of Degraded Ecosystems, South China Botanical Garden, Chinese Academy of Sciences (VRMDE2202), and the Hydraulic science and technology innovation project of Guangdong Province (Project No. 2020–09).

Appendix A. Supplementary data

Supplementary data to this article can be found online at https://doi.org/10.1016/j.jclepro.2022.135749.

References

Anderson, D.M., Glibert, P.M., Burkholder, J.M., 2002. Harmful algal blooms and eutrophication: nutrient sources, composition, and consequences. Estuaries 25, 704–726.
Andrén, E., Telford, R.J., Jonsson, P., 2017. Reconstructing the history of eutrophication and quantifying total nitrogen reference conditions in Bothnian Sea coastal waters. Estuar. Coast Shelf Sci. 198, 320–328.
Andrews, J.E., Greenaway, A.M., Dennis, P.F., 1998. Combined carbon isotope and C/N ratios as indicators of source and fate of organic matter in a poorly flushed, tropical estuary: Hunts Bay, Kingston Harbour, Jamaica. Estuarine. Coast. Shelf Sci. 46, 743–756.
Appleby, P., 2002. Chronostratigraphic Techniques in Recent Sediments, Tracking Environmental Change Using Lake Sediments. Springer, Dordrecht, pp. 171–203.
Beegle, D.B., Carton, O.T., Bailey, J.S., 2000. Nutrient management planning: justification, theory, practice. J. Environ. Qual. 29, 72–79.
Bing, H., Wu, Y., Zhou, J., Li, R., Wang, J., 2016. Historical trends of anthropogenic metals in Eastern Tibetan Plateau as reconstructed from alpine lake sediments over the last century. Chemosphere 148, 211–219.
Bricker, S.B., Ferreira, J.G., Zhu, C., Rose, J.M., Galimany, E., Wikfors, G., Saurel, C., Miller, R.L., Wands, J., Trowbridge, P., Grizzle, R., Wellman, K., Rheault, R., Steinberg, J., Jacob, A., Davenport, E.D., Ayvazian, S., Chintala, M., Tedesco, M.A., 2018. Role of shellfish aquaculture in the reduction of eutrophication in an urban estuary. Environ. Sci. Technol. 52, 173–183.
Bricker, S.B., Grizzle, R.E., Trowbridge, P., Rose, J.M., Ferreira, J.G., Wellman, K., Zhu, C., Galimany, E., Wikfors, G.H., Saurel, C., Miller, R.L., Wands, J., Rheault, R., Steinberg, J., Jacob, A.P., Davenport, E.D., Ayvazian, S., Chintala, M., Tedesco, M.A., 2020. Bioextractive removal of nitrogen by oysters in great Bay Piscataqua River Estuary, New Hampshire, USA. Estuar. Coast 43, 23–38.
Canfield, D.E., Bjerrum, C.J., Zhang, S., Wang, H., Wang, X., 2020. The modern phosphorus cycle informs interpretations of Mesoproterozoic Era phosphorus dynamics. Earth Sci. Rev. 208, 103267.
Canfield, D.E., Kristensen, E., Thamdrup, B., 2005. Aquatic Geomicrobiology. Elsevier.

Chen, P.F., Zhang, R.J., Du, Z.L., Wang, G.H., Dong, H.T., Cui, B., Fan, R.P., Li, L.X., Wang, Q.B., Liu, Y.S., Sun, Z.M., 2022. Microbial composition and nitrogen removal pathways in a novel sequencing batch reactor integrated with semi-fixed biofilm carrier: evidence from a pilot study for low- and high-strength sewage treatment. Environ. Sci. Pollut. Control Ser. 29, 49105–49115.
Collins, A.L., Burak, E., Harris, P., Pulley, S., Cardenas, L., Tang, Q., 2019. Field scale temporal and spatial variability of δ13C, δ15N, TC and TN soil properties: implications for sediment source tracing. Geoderma 333, 108–122.
Conley, D.J., Paerl, H.W., Howarth, R.W., Boesch, D.F., Seitzinger, S.P., Havens, K.E., Christiane, L., Likens, G.E., 2009. Controlling eutrophication: nitrogen and phosphorus. Science 323, 1014–1015.
Conrad, S.R., Santos, I.R., Brown, D.R., Sanders, L.M., van Santen, M.L., Sanders, C.J., 2017. Mangrove sediments reveal records of development during the previous century (Coffs Creek estuary, Australia). Mar. Pollut. Bull. 122, 441–445.
Dai, J., Song, J., Li, X., Yuan, H., Li, N., Zheng, G., 2007. Environmental changes reflected by sedimentary geochemistry in recent hundred years of Jiaozhou Bay, North China. Environ. Pollut. 145, 656–667.
Dai, Z., Du, J., Zhang, X., Su, N., Li, J., 2011. Variation of riverine material loads and environmental consequences on the Changjiang (Yangtze) Estuary in recent decades (1955– 2008). Environ. Sci. Technol. 45, 223–227.
de Mulder, E.F.J., van Bruchem, A.J., Claessen, F.A.M., Hannink, G., Hulsbergen, J.G., Satijn, H.M.C., 1994. Environmental impact assessment on land reclamation projects in The Netherlands: a case history. Eng. Geol. 37, 15–23.
Dick, W.A., Tabatabai, M.A., 1977. Determination of orthophosphate in aqueous solutions containing labile organic and inorganic phosphorus compounds. J. Environ. Qual. 6, 82–85.
Ding, S., Wang, Y., Wang, D., Li, Y., Gong, M., Zhang, C., 2016. In situ, high-resolution evidence for iron-coupled mobilization of phosphorus in sediments. Sci. Rep. 6, 1–11.
Ellegaard, M., Clarke, A.L., Reuss, N., Drew, S., Weckström, K., Juggins, S., Anderson, N. J., Conley, D.J., 2006. Multi-proxy evidence of long-term changes in ecosystem structure in a Danish marine estuary, linked to increased nutrient loading. Estuar. Coast Shelf Sci. 68, 567–578.
Gao, L., Wang, Z., Shan, J., Chen, J., Tang, C., Yi, M., 2017. Aquatic environmental changes and anthropogenic activities reflected by the sedimentary records of the Shima River, Southern China. Environ. Pollut. 224, 70–81.
Golterman, H.L., 2007. The Chemistry of Phosphate and Nitrogen Compounds in Sediments. Springer, Dordrecht.
Greening, H., Janicki, A., Sherwood, E.T., Pribble, R., Johansson, J.O.R., 2014. Ecosystem responses to long-term nutrient management in an urban estuary: Tampa Bay, Florida, USA. Estuarine. Coast. Shelf Sci. 151, A1–A16.
Guo, Y., Yang, S., 2016. Heavy metal enrichments in the Changjiang (Yangtze River) catchment and on the inner shelf of the East China Sea over the last 150 years. Sci. Total Environ. 543, 105–115.
Heisler, J., Glibert, P.M., Burkholder, J.M., Anderson, D.M., Cochlan, W., Dennison, W. C., Dortch, Q., Gobler, C.J., Heil, C.A., Humphries, E., 2008. Eutrophication and harmful algal blooms: a scientific consensus. Harmful Algae 8, 3–13.
Hieltjes, A.H.M., Lijklema, L., 1980. Fractionation of inorganic phosphates in calcareous sediments. J. Environ. Qual. 9, 405–407.
Hu, J., Peng, P.a., Jia, G., Mai, B., Zhang, G., 2006. Distribution and sources of organic carbon, nitrogen and their isotopes in sediments of the subtropical Pearl River estuary and adjacent shelf, Southern China. Mar. Chem. 98, 274–285.
Huang, X.P., Huang, L.M., Yue, W.Z., 2003. The characteristics of nutrients and eutrophication in the Pearl River estuary, South China. Mar. Pollut. Bull. 47, 30–36.
Ip, C.C.M., Li, X.D., Zhang, G., Farmer, J.G., Wai, O.W.H., Li, Y.S., 2004. Over one hundred years of trace metal fluxes in the sediments of the Pearl River Estuary, South China. Environ. Pollut. 132, 157–172.
Irizuki, T., Hirose, K., Ueda, Y., Fujihara, Y., Ishiga, H., Seto, K., 2018. Ecological shifts due to anthropogenic activities in the coastal seas of the Seto Inland Sea, Japan, since the 20th century. Mar. Pollut. Bull. 127, 637–653.
Jia, G., Peng, P., 2003. Temporal and spatial variations in signatures of sedimented organic matter in Lingding Bay (Pearl estuary), southern China. Mar. Chem. 82, 47–54.
Jiang, L., 1995. Changing kinship structure and its implications for old-age support in urban and rural China. Popul. Stud. 49, 127–145.
Jordan, T.E., Cornwell, J.C., Boynton, W.R., Anderson, J.T., 2008. Changes in phosphorus biogeochemistry along an estuarine salinity gradient: the iron conveyer belt. Limnol. Oceanogr. 53, 172–184.
Kabir, T., De Laporte, A., Nasielski, J., Weersink, A., 2021. Adjusting nitrogen rates with split applications: modelled effects on N losses and profits across weather scenarios. Eur. J. Agron. 129.
Koster, D., Lichter, J., Lea, P.D., Nurse, A., 2007. Historical eutrophication in a river-estuary complex in mid-coast Maine. Ecol. Appl. 17, 765–778.
Lee, C.-H., Lee, B.-Y., Chang, W.K., Hong, S., Song, S.J., Park, J., Kwon, B.-O., Khim, J.S., 2014. Environmental and ecological effects of Lake Shihwa reclamation project in South Korea: a review. Ocean Coast Manag. 102, 545–558.
Li, J., Zheng, B., Hu, X., Wang, Y., Ding, Y., Liu, F., 2015. Terrestrial input and nutrient change reflected by sediment records of the Changjiang River Estuary in recent 80 years. Acta Oceanol. Sin. 34, 27–35.
Li, R., Tang, C., Li, X., Jiang, T., Shi, Y., Cao, Y., 2019. Reconstructing the historical pollution levels and ecological risks over the past sixty years in sediments of the Beijiang River, South China. Sci. Total Environ. 649, 448–460.
Liu, G.Q., Zhang, G., Li, X.D., Li, J., Peng, X.Z., Qi, S.H., 2005. Sedimentary record of polycyclic aromatic hydrocarbons in a sediment core from the Pearl River Estuary, South China. Mar. Pollut. Bull. 51, 912–921.
Liu, H., Chen, Y.D., Liu, T., Lin, L., 2019. The River Chief system and river pollution control in China: a case study of Foshan. Water 11, 1606.
Liu, Q., Liang, Y., Cai, W., Wang, K., Wang, J., Yin, K., 2020. Changing riverine organic C:N ratios along the Pearl River: implications for estuarine and coastal carbon cycles. Sci. Total Environ. 709, 136052.
Liu, Z., Fagherazzi, S., Cui, B., 2021a. Success of coastal wetlands restoration is driven by sediment availability. Commun. Earth Environ. 2.
Liu, Z., Fagherazzi, S., Li, J., Cui, B., 2021b. Mismatch between watershed effects and local efforts constrains the success of coastal salt marsh vegetation restoration. J. Clean. Prod. 292.
Meyers, P.A., 1994. Preservation of elemental and isotopic source identification of sedimentary organic matter. Chem. Geol. 114, 289–302.
Némery, J., Garnier, J., 2016. The fate of phosphorus. Nat. Geosci. 9, 343–344.
Parsons, C.T., Rezanezhad, F., O'Connell, D.W., Van Cappellen, P., 2017. Sediment phosphorus speciation and mobility under dynamic redox conditions. Biogeosciences 14, 3585–3602.
Qian, H., Liang, S., 1999. Study on the red tide in the Pearl River Estuary and its near waters (in Chinese). Mar. Environ. Sci. 18, 69–74.
Redfield, A.C., 1958. The biological control of chemical factors in the environment. Am. Sci. 46 (230A), 205–221.
Roy, E.D., Nguyen, N.T., White, J.R., 2017. Changes in estuarine sediment phosphorus fractions during a large-scale Mississippi River diversion. Sci. Total Environ. 609, 1248–1257.
Sellner, K.G., Doucette, G.J., Kirkpatrick, G.J., 2003. Harmful algal blooms: causes, impacts and detection. J. Ind. Microbiol. Biotechnol. 30, 383–406.
Sterner, R.W., Elser, J.J., 2003. The Biology of Elements from Molecules to the Biosphere, Ecological Stoichiometry. Princeton University Press, Princeton, p. 439.
Velinsky, D.J., Paudel, B., Sommerfield, C.K., 2020. Long-term sediment accretion and nutrient deposition in a tidal marsh of the Delaware Bay. Proc. Acad. Nat. Sci. Phila. 167, 87–103.
Wang, Z., Feng, J., Nie, X., 2015. Recent environmental changes reflected by metals and biogenic elements in sediments from the Guishan Island, the Pearl River Estuary, China. Estuarine. Coast. Shelf Sci. 164, 493–505.
Xuan, Y., Tang, C., Liu, G., Cao, Y., 2020. Carbon and nitrogen isotopic records of effects of urbanization and hydrology on particulate and sedimentary organic matter in the highly urbanized Pearl River Delta, China. J. Hydrol. 591, 125565.
Yamamoto, T., 2003. The Seto Inland Sea—eutrophic or oligotrophic? Mar. Pollut. Bull. 47, 37–42.
Ye, F., Huang, X., Zhang, D., Tian, L., Zeng, Y., 2012. Distribution of heavy metals in sediments of the Pearl River Estuary, Southern China: implications for sources and historical changes. J. Environ. Sci. 24, 579–588.
Ye, Z., Chen, J., Gao, L., Liang, Z., Li, S., Li, R., Jin, G., Shimizu, Y., Onodera, S.-i., Saito, M., Gopalakrishnan, G., 2020. (210)Pb dating to investigate the historical variations and identification of different sources of heavy metal pollution in sediments of the Pearl River Estuary, Southern China. Mar. Pollut. Bull. 150, 110670.
Yin, K., Qian, P., Chen, J.C., Hsieh, D.P.H., Harrison, P.J., 2000. Dynamics of nutrients and phytoplankton biomass in the Pearl River estuary and adjacent waters of Hong Kong during summer: preliminary evidence for phosphorus and silicon limitation. Mar. Ecol. Prog. Ser. 194, 295–305.
Yu, F., Zong, Y., Lloyd, J.M., Huang, G., Leng, M.J., Kendrick, C., Lamb, A.L., Yim, W.W. S., 2010. Bulk organic δ13C and C/N as indicators for sediment sources in the Pearl River delta and estuary, southern China. Estuarine. Coast. Shelf Sci. 87, 618–630.
Zhang, G., Cheng, W., Chen, L., Zhang, H., Gong, W., 2019. Transport of riverine sediment from different outlets in the Pearl River Estuary during the wet season. Mar. Geol. 415, 105957.
Zhang, L., Yin, K., Wang, L., Chen, F., Zhang, D., Yang, Y., 2009a. The sources and accumulation rate of sedimentary organic matter in the Pearl River Estuary and adjacent coastal area, Southern China. Estuarine. Coastal Shelf Sci. 85, 190–196.
Zhang, S., Yi, Q., Buyang, S., Cui, H., Zhang, S., 2020. Enrichment of bioavailable phosphorus in fine particles when sediment resuspension hinders the ecological restoration of shallow eutrophic lakes. Sci. Total Environ. 710, 135672.
Zhang, Y., Wang, Y., Wang, Y., Xi, H., 2009b. Investigating the impacts of landuse-landcover (LULC) change in the Pearl River Delta region on water quality in the Pearl River Estuary and Hong Kong's coast. Rem. Sens. 1, 1055–1064.
Zhao, Y., Wu, R., Cui, J., Gan, S., Pan, J., Guo, P., 2020. Improvement of water quality in the Pearl River Estuary, China: a long-term (2008–2017) case study of temporal-spatial variation, source identification and ecological risk of heavy metals in surface water of Guangzhou. Environ. Sci. Pollut. Res. 27, 21084–21097.
Zhou, H., Peng, X., Pan, J., 2004. Distribution, source and enrichment of some chemical elements in sediments of the Pearl River Estuary, China. Continent. Shelf Res. 24, 1857–1875.